International Journal of Heat and Mass Transfer 149 (2020) 119246

Contents lists available at ScienceDirect

International Journal of Heat and Mass Transfer

journal homepage: www.elsevier.com/locate/hmt

Three-dimensional numerical simulation of saturated annular flow boiling in a narrow rectangular microchannel

Yang Luo[a], Wei Li[a,*], Kan Zhou[a], Kuang Sheng[b], Shuai Shao[b], Zhengjiang Zhang[a], Jingcai Du[a], W.J. Minkowycz[c]

[a] Department of Energy Engineering, Zhejiang University, Hangzhou 310027, China
[b] College of Electrical Engineering, Zhejiang University, Hangzhou, 310027, China
[c] Department of Mechanical and Industrial Engineering (M/C 251), University of Illinois at Chicago, 842 West Taylor Street, Room 2049 ERF 60607-7022, Chicago, IL, United States

ARTICLE INFO

Article history:
Received 20 September 2019
Revised 7 December 2019
Accepted 16 December 2019
Available online xxx

Keywords:
Narrow microchannel
Volume of fluid method
Saturated flow boiling
Annular flow
Numerical simulation

ABSTRACT

A fundamental numerical investigation on hydrodynamics and heat transfer performance of annular flow boiling in a rectangular microchannel with large width-to-depth ratio is performed in the paper. The saturation temperature recovery model based on the volume of fluid (VOF) method is implemented in OpenFOAM package to explore the heat transfer characteristics in annular flow regime with a three-dimensional computational domain. Validation of our methods has been conducted by comparing numerical results with experimental data. Effects of operating conditions including inlet mass flux, wall heat flux and inlet vapor quality are further discussed. It is found that the increase in wall heat flux or inlet quality will lead to the decrease of liquid thin film thickness between the interface and the heating wall. As the interfacial temperature is fixed at the saturation temperature, thinner liquid film will result in larger local heat transfer coefficient and lower wall temperature, which improves the heat transfer performance of the narrow microchannel. However, increasing the inlet mass flux will decrease the wall heat transfer coefficient, which is in accordance with the experimental result.

1. Introduction

At present, with rapid development in power output and miniaturization trend of size, weight as well as cost for various electronic devices, tremendous heat flux needs to be dissipated effectively. For example, the average heat flux of today's high-performance computer chips is expected to reach 2–4.2 MW/m^2. While in insulated gate bipolar translator (IGBT) chips, the heat flux density could be as high as 6.5 MW/m^2 [1]. Thus, nowadays traditional single-phase cooling schemes such as natural air convection and forced liquid convection are no longer satisfactory when faced with the constraints coming from operation safety requirements and manufacture techniques. Since the phase change process can use the latent heat of vaporization, the heat transfer coefficient (HTC) of flow boiling is much higher than that of the single phase. With additional advantages of higher surface to volume ratio and less demand for working fluid consumption, microchannel heat sinks utilizing boiling is considered to be one of the most promising methods to solve the thermal management problems of next-generation electronic devices with high heat flux dissipation. Although microchannel heat exchangers of multiphase flow are widely studied and used in industry and academia, there are still many shortcomings and lack of understanding as for research work of flow and heat transfer characteristics of flow boiling in microchannels, which hinder its corresponding applications. Due to the weakened influence of gravity, other interfacial forces such as surface tension force and shear stress become more dominated for the flow pattern evolution and the heat transfer characteristics in microchannels, which are distinctly different from those of conventional channels [2].

In recent decades, substantial experiment and numerical investigations related to two phase flow in microchannels have been carried out, covering various working fluids such as water, dielectric solvents and refrigerants, different mass flow rates and heat flux densities, in single or multi-port parallel channels with various cross-sectional geometries including circular, rectangular, trapezoidal and triangular microchannels. Among those experimental investigations, Wu and Li [3] proposed a critical criterion for distinguishing the two phase flow in the microchannel to the conventional channel based on the dimensionless number

* Corresponding author: Department of Energy Engineering, Zhejiang University, Hangzhou 310027, China.
E-mail address: weili96@zju.edu.cn (W. Li).

https://doi.org/10.1016/j.ijheatmasstransfer.2019.119246
0017-9310/

Nomenclature

A_{ch}	Cross-sectional area, m^2
c_p	Specific heat, kJ/kg °C
$\boldsymbol{f}_\sigma$	Surface tension body force, N/m^3
G	Mass flux, kg/m^2s
$\boldsymbol{g}$	Gravitational acceleration, m/s^2
h	Heat transfer coefficient, $W/m^2°C$
i	Specific enthalpy, kJ/kg
i_{lv}	Latent heat of vaporization, kJ/kg
k	Thermal conductivity, W/m °C
L	length of the rectangular for inlet phase distribution, m
$\boldsymbol{n}$	Normal vector to surface
p	Pressure, Pa
$\dot{q}_{lv}$	Volumetric phase change source term, W/m^3
q_w	Wall heat flux, W/m^2
R	Radius of the semicircular for inlet phase distribution, m
T	Temperature, °C
t	Time, s
$\boldsymbol{u}$	Instantaneous velocity, m/s
$\dot{v}_{\mathrm{lv}}$	Volumetric evaporation rate, 1/s
x_{in}	Inlet vapor quality

Greek letters

α	Volume fraction
$\dot{\alpha}_{\mathrm{lv}}$	Phase-fraction generation rate, 1/s
δ	Liquid film thickness, m
ε	Void fraction
κ	Interface curvature, 1/m
μ	Dynamic viscosity, kg/ms
ρ	Density, kg/m^3
σ	Surface tension coefficient, N/m
φ	Thermophysical property (ρ, μ, k)

Subscripts

ave	Average value
exp	Experimental value
in	Inlet
l	Liquid phase
lv	Liquid-vapor phase change
ref	Reference value
sim	Simulation data
v	Vapor phase
w	Wall
x	Coordinate in x-direction
y	Coordinate in y-direction
z	Coordinate in z-direction

groups consisted of *Bo* (Bond Number) and *Re* (Reynolds Number), and further developed a series of heat transfer coefficient, pressure drop gradient and critical heat flux prediction correlations fitted through the collected microchannel flow boiling experimental databases [4–6]. Costa-Patry and Thome [7] proposed a brand new flow-regime-based unified modeling suite according to their recent experimental results for multi-microchannel evaporators and single-microchannel tubes, which could predict and capture the heat transfer characteristics of slug flow and annular flow. Thome et al. [8] further summarized empirically-validated flow regime maps for mini- and micro-channels in the literature. Harirchian and Garimella [9–11] have performed a comprehensive study on the hydraulic and thermal transport characteristics of flow boiling in multi-port parallel microchannels, which covered the influence of various channel geometry parameters under different test conditions. Alam et al. [12] measured the flow boiling heat transfer, pressure drop and instability characteristics of micro-gap heat sinks, which were compared against parallel microchannels with the identical flow passage area.

The main drawback of experimental investigations lies in that high-resolution diagnostic tools are required to obtain qualitative and quantitative descriptions about the behavior of nucleated boiling and interfacial evaporation at the microscale, accompanied with comprehensive multi-physics and multi-process information. Recently particle image or tracing velocimetry based laser diagnostics, infrared thermometry and high speed camera as well as coupled image processing technique have been implemented to allow simultaneous interface tracking, liquid-field velocity and temperature, and wall temperature measurements in the few research work available. Barber et al. [13] studied the bubble confinement behaviors of FC-72 flow boiling in a rectangular microchannel with dimensions of 4.0 × 0.4 mm^2, in which bubble nucleation and growth processes with accompanied periodic elongation bubble formation was observed through visualization techniques. Similarly, the bubble dynamics in multi-port parallel microchannels and their effects on flow instability and heat transfer characteristics was investigated by Bogojevic et al. [14] with aid of the high-speed camera and coupled microscope. It was concluded that bubble confinement and interactions between channels affected flow structures significantly. Huang et al. studied the instantaneous substrate temperature response characteristics of R236fa and R245fa flow boiling in various parallel microchannel test pieces under transient heat loads, which was monitored using an infrared (IR) camera [15]. By depositing a total of 53 platinum-based thin film resistance thermal resistors under the silicon substrate, highly-resolved wall temperatures were measured in the experimental work of Bigham and Moghaddam [16] to study the flow boiling heat transfer mechanism of FC-72 in a single microchannel with structured micropillar arrays. Meanwhile, micro-resolution particle image velocimetry (μPIV) technique was employed by Wang et al. [17] to measure the boiling hydrodynamics characteristics on hydrophobic Teflon cylinders constructed around the hydrophilic substrate. Piasecka et al. [18] used liquid crystal and infrared thermography to record the outer surface and inside wall temperatures of FC-72 flow boiling in vertical mini-channels.

At the same period, numerical methods have been more and more widely used in the study of vapor bubble dynamics, two-phase flow regime transition and heat transfer characteristics of flow boiling in macro-/micro-channels. Since finer local heat transfer coefficient, velocity/temperature field and phase interface distribution could be obtained, a large number of numerical investigations have been reported to investigate the heat and mass transfer processes of flow boiling in recent decades. The empirical phase change rate parameter model of Lee [19] based on the VOF multiphase flow method were used to numerically perform the flow boiling of R141b in a horizontal coiled tube, and the corresponding experimental heat transfer characteristics measurements as well as flow pattern visualization were also conducted and compared [20]. The two-fluid approach and the wall boiling partitioning model coupled with several sub-models was implemented in the CFX code by Yang et al. [21] to simulate the subcooled boiling thermal-hydraulics in the vertical rectangular narrow channel. Mukherjee and Kandlikar [22] numerically studied the growth process of nucleated bubbles in a square microchannel with boundary conditions of superheated fluid bulk and constant wall temperature through the level set (LS) method and the sharp interface phase change model. Subsequently, Mukherjee et al. [23] further studied the effects of surface tension and contact angles on the bubble evolution behaviors and heat transfer characteristics near wall. Zhuan and Wang [24] numerically studied flow pattern transitions for saturated boiling of R134a and R22 in circular micro-tubes, in

which the bubble growth and coalescence characteristics of bubbly flow, slug flow and annular flow were investigated. Through combination of the VOF method and the saturation temperature recovery model [25], Luo et al. [26] studied effects of boundary conditions such as the heat flux, contact angle, surface tension and inlet Reynolds number on the bubble dynamics for growth of single nucleated bubble and coalescence of adjacent bubbles. Ferrari et al. [27] conducted a CFD investigation on flow boiling heat transfer characteristics of R245fa during the slug flow regime in a square microchannel, and effects of the channel cross-sectional geometry (circular or square) were studied. Lorenzini and Joshi [28] used a three-dimensional VOF model coupled with the phase change model of Lee to explore effects of the non-uniform heat flux and refrigerant flow rate on the cooling performance in microelectronics.

The annular flow regime is characterized by a continuous vapor core at the center of the channel cross section, which traps a thin layer of liquid against the surrounding walls. The liquid-vapor interface and surrounding annular liquid film distribution is of fundamental importance during the annular flow boiling process since thickness of the liquid film beneath central vapor core determines the local heat transfer performance [29]. Even though slug flow and annular flow are the most expected flow pattern at the microscale [30,31], few CFD investigations are performed towards annular liquid film evaporation in microchannels due to the complexity nature in simulating annular flow numerically, including several one dimensional mathematical procedures [32–34] or two dimensional axisymmetric computational models [35,36]. Nowadays square or rectangular cross-sectional shape are more common geometries encountered in practice, so three-dimensional simulation of annular flow boiling in rectangular microchannel is performed in this study.

Na and Chung [34] obtained the velocity and temperature distribution of annular flow in the circular microchannel based on a two-dimensional axisymmetric model, and calculated thickness of the annular liquid film considering the disjoining pressure and surface tension effects for constant heat flux and wall temperature boundary conditions. Jesseela and Sobhan [37] numerically solved a quasi-three-dimensional mathematical model and studied the fluid flow and heat transfer characteristics of annular flow in rectangular microchannels with different hydraulic diameters. By using the self-developed FORTRAN code to solve governing equations, effects of heat flux, mass flow rate and channel geometry on the velocity filed, phase distribution and pressure drop were studied by Patel et al. [38], which took effects of the shear stress, gravity acceleration, surface tension and phase interface curvature into consideration. Two-dimensional axisymmetric CFD model was utilized by Guo et al. [36] to analyze the interfacial instability characteristics of laminar isothermal fully developed annular flow in circular microchannels with natural or imposed inlet perturbation. Later on, flow boiling hydrodynamics and thermodynamics of annular flow in microchannels was studied and parametric numerical analysis was carried out to investigate effects of the channel geometry, system pressure, mass flux, wall heat flux and vapor quality on the heat transfer performance [35].

In our previous numerical simulations [26,39,40], phase change investigations including steady-state annular flow condensation or bubbly/slug flow boiling in mini-/micro-scale tubes and microchannels had been comprehensively conducted using numerical methods. Experimental investigations for flow boiling in rectangular microchannels were also widely explored [41–43]. In the present study, saturation temperature recovery model for phase change based on the VOF method is implemented in the OpenFOAM [44,45] package to explore the heat and mass transfer characteristics of annular flow regime in a single rectangular microchannel using a three-dimensional computational domain. As far as we know, this is the first attempt to perform a three-dimensional numerical simulation of annular flow boiling. Cases of validation are performed by comparing the numerical results with our own experimental data. Effects of operating conditions including inlet mass flux, wall heat flux and inlet vapor quality on corresponding heat transfer coefficients and flow patterns are further discussed.

2. Numerical methods

2.1. Governing equations

In this section, details of mathematical models and numerical methods for this study are elaborated. The numerical investigation on two-phase flow is based on the compressive VOF method implemented in the OpenFOAM package. For incompressible and immiscible Newtonian fluids with low Mach number, basic equations based on the finite volume method can be written as:

VOF equation:

$$\frac{\partial \alpha}{\partial t} + \nabla \cdot (\mathbf{u}^* \alpha) = \dot{\alpha}_{lv} \tag{1}$$

Mass conservation:

$$\nabla \cdot \mathbf{u} = \dot{v}_{\mathrm{lv}} \tag{2}$$

Momentum equation:

$$\frac{\partial (\rho \mathbf{u})}{\partial t} + \nabla \cdot (\rho \mathbf{u}\mathbf{u}) = \mathbf{f}_\sigma - \nabla p + \nabla \cdot \left\{ \mu \left[\nabla \mathbf{u} + (\nabla \mathbf{u})^T \right] \right\} + \rho \mathbf{g} \tag{3}$$

Energy conservation equation:

$$\frac{\partial (\rho i)}{\partial t} + \nabla \cdot (\rho \mathbf{u} i) = \nabla \cdot (k \nabla T) - \dot{q}_{lv} \tag{4}$$

In the VOF equation, the volume fraction function α is introduced for phase distribution in the domain. When $\alpha = 1$ the mesh cell center is considered full of pure liquid while $\alpha = 0$ indicates pure vapor phase. Since working fluid used in this study is considered as incompressible, constant fluid thermophysical properties including conductivity, viscosity and density are adopted. The properties are evaluated using volume-fraction weighted value:

$$\varphi = (1 - \alpha) \cdot \varphi_v + \alpha \cdot \varphi_l \tag{5}$$

where:

$$\varphi \in \{\rho, \mu, k\} \tag{6}$$

For the reason that specific heats are assumed constant for both liquid and vapor phase, the fluid enthalpy can be evaluated as:

$$i = \frac{(1 - \alpha)\rho_v c_{p,v} + \alpha \rho_l c_{p,l}}{\rho} \left(T - T_{ref} \right) \tag{7}$$

Note that the compression velocity field $\boldsymbol{u}^*$ in Eq. (1) is added to counteract the numerical diffusion of α in the vicinity of liquid-vapor interface [44]. Details of this technique can be found in the literature [46,47].

Surface tension and gravitational forces are introduced in the momentum equation. The surface tension force on liquid-vapor interface is regarded as an additional source term $\mathbf{f}_\sigma$ according to Brackbill's continuum surface force (CSF) model [48]. Marangoni effect caused by the variation of surface tension coefficient is not taken into consideration in this study [39]. A multiplier term $2\rho/(\rho_v+\rho_l)$ is employed on the right hand side of Eq. (8) so that the surface tension source term is proportional to the average density [48].

$$\mathbf{f}_\sigma = \sigma \kappa \mathbf{n} |\nabla \alpha| \frac{2\rho}{\rho_v + \rho_l} \kappa = -(\nabla \cdot \mathbf{n})\mathbf{n} = \frac{\nabla \alpha}{|\nabla \alpha|} \tag{10}$$

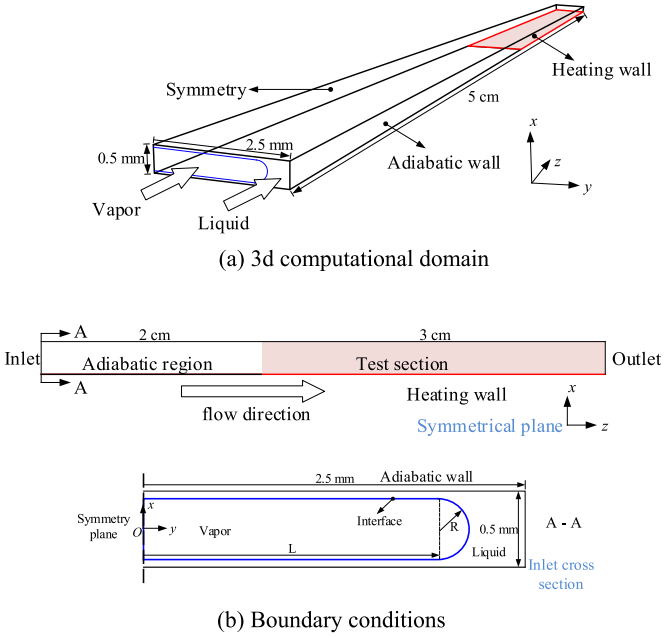

Fig. 1. Three-dimensional computational domain and boundary conditions. (a) 3d computational domain, (b) Boundary conditions.

2.2. Modeling of source term

To simulate interactions of mass, momentum and energy transfer processes between liquid and vapor phases, source terms are added into equations. On basis of VOF method, phase change models such as Lee model [49], sharp interface model [50] and Schrage model [51] can be used for evaluating the evaporation rate. Otherwise, kinds of experimentally developed or analytical heat transfer correlations [52] were also proposed in the past.

Here, the saturation temperature recovery model proposed by Rattner et al. [53] is conducted to perform interfacial evaporation of annular flow in microchannel. Constant saturated temperature is set at the liquid-vapor interface cells at each time step. Before determining the volumetric evaporation rate $\dot{v}_{lv}$ and the phase-fraction generation rate $\dot{\alpha}_{lv}$ in Eqs. (1),(2), the volumetric phase-change heating rate $\dot{q}_{lv}$ should be evaluated as:

$$\dot{q}_{lv} = min\left[\frac{\rho i}{\Delta t}, \frac{\alpha_l \rho_l i_{lv}}{\Delta t}, \frac{i_{lv}}{\Delta t}/\left(\frac{1}{\rho_v} - \frac{1}{\rho_l}\right)\right] \tag{11}$$

Then the volumetric evaporation rate $\dot{v}_{lv}$ and the phase-fraction generation rate $\dot{\alpha}_{lv}$ for solving Eqs. (1) and (2) can be calculated explicitly:

$$\dot{\alpha}_{lv} = -\frac{\dot{q}_{lv}}{\rho i_{lv}}\dot{v}_{lv} = \frac{\dot{q}_{lv}}{i_{lv}}\left(\frac{1}{\rho_v} - \frac{1}{\rho_l}\right) \tag{13}$$

Detailed descriptions of this phase change model have been discussed in Refs. [25,39].

3. Numerical validation

3.1. Computational domain and boundary conditions

Fig. 1(a) and (b) shows the computational domain and boundary conditions for simulating annular flow boiling process in a narrow rectangular microchannel, which is similar to the experimental setup. A three-dimensional rectangular microchannel is used with dimensions of 0.5 × 5 mm^2 (depth × width), as depicted in Fig. 1(a). The narrow microchannel consists of a 20 mm adiabatic section and a 30 mm test section with a heating wall.

Table 1
Material properties of water.

	Vapor	Liquid
Kinematic viscosity (m^2/s)	2.0449 × 10^{-5}	2.9382 × 10^{-7}
Density (kg/m^3)	0.59817	958.35
Thermal conductivity (W/m °C)	0.025096	0.67909
Specific heat (J/kg °C)	2080.0	4215.7
Saturation temperature (°C)	100	
Latent heat of vaporization (kJ/kg)	2256.4	

Details of boundary conditions applied in the computational domain are illustrated in Fig. 1(b). Considering that the gravitational acceleration is along the negative direction of the z axis, symmetry boundary condition can be set for the x-z plane in middle of the channel cross section as show in Fig. 1(a). Therefore, only half of the channel need to be modeled. No-slip wall boundary condition is applied for channel walls. Additionally, a uniform wall heat flux is imposed on the heating wall while other walls are adiabatic, which is in accordance with the experimental setup. To obtain a steady annular flow regime in the high-aspect-ratio microchannel, a special inlet phase distribution boundary condition is used. As depicted in Fig. 1(b), the vapor core is assumed as a combination of a rectangle ($L \times 2R$) and a semicircle at the inlet. It should be noted that radius of the semicircle R is kept at 0.24 mm for all cases while the length of the rectangle L in Fig. 1(b) can be calculated based on the inlet void fraction ε. Because the inlet vapor quality x_{in} has been given by the experiments, the empirical void fraction model for annular flow in microchannel proposed by Cioncolini and Thome [54] is used to calculate the phase distribution at the inlet boundary. The void fraction ε at the inlet entrance can be derived as follows:

$$\varepsilon = \frac{a \cdot x_{in}^b}{1 + (a-1) \cdot x_{in}^b} \tag{14}$$

where:

$$a = -2.129 + 3.129 \times \left(\rho_v \cdot \rho_l^{-1}\right)^{-0.2186} \tag{15}$$

$$b = 0.3487 + 0.6513 \times \left(\rho_v \cdot \rho_l^{-1}\right)^{-0.5150} \tag{16}$$

After determining the distribution of phases, the average velocity of both liquid and vapor phases at the inlet entrance can be estimated using the given mass flux and inlet vapor quality under various test cases. After passing through the adiabatic entrance section, the annular flow is considered as hydrodynamically fully developed.

Fluids at saturation temperature ($T_{in} = T_{sat} = 100$ °C) with the fixed vapor quality x flowed into the adiabatic section and the test section successively. It should be noted that evaporation occurred on the liquid-vapor interface in the heated section but there is no liquid film dryout according to the experimental observation. Water is used as the working fluid in this numerical study, constant properties of liquid and vapor are queried through the NIST REFPROP 9.0, as shown in Table 1.

3.2. Mesh independence analysis

Prior to the numerical investigation of annular flow boiling in the microchannel, mesh independence analysis is performed to find a moderate mesh scheme for balancing the numerical cost and accuracy. Structural grids of orthogonal hexahedral elements are generated to discretize the computational domain. Uniform mesh in the z direction and a gradually refined mesh in the near-wall region are used to capture the evaporating liquid film underneath the central vapor column. As shown in Fig. 2, at least five cells suggested by Gupta et al. [55] is guaranteed for near-wall region.

Table 2
Grid independence test.

No.	$x \times y \times z$	Near-wall region cell thickness (μm)	Element numbers
1	16 × 25 × 125	3.33	50,000
2	16 × 50 × 125	3.33	100,000
3	30 × 50 × 125	2	187,500
4	40 × 50 × 125	1.25	250,000
5	40 × 100 × 125	1.25	500,000
6	40 × 100 × 250	1.25	1,000,000

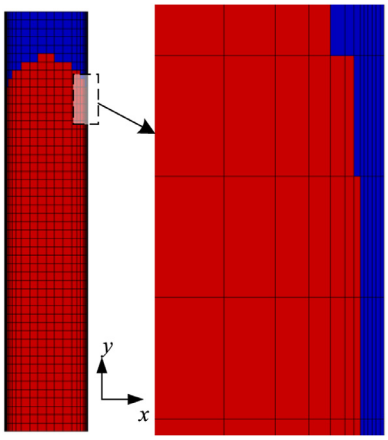

Fig. 2. Mesh distribution of channel cross section.

Fig. 3(a) shows the mesh independence test results in terms of the time- and area-averaged wall superheat. Note that the values of wall temperature are time- and area-averaged after the flow reaches the quasi-steady state. The total flow time simulated was 2 s and we found the average temperature on the heated wall became stable after 1 s. Therefore, the numerical data for comparison is calculated with simulated time ranging from 1 s to 2 s. Six different number of mesh schemes listed in Table 2 are used under a given operating condition based on the experimental research. The surface-averaged temperature on the entire heating wall and the average temperature of four specific locations are compared with the experimental data. In experiments, there is four thermocouple probes placed under the test section [43] at the distances of 7.5 mm, 12.5 mm, 17.5 mm and 22.5 mm from front edge of the test section along the flow direction. There is less than 2% variation of average superheats if the number of mesh element is larger than 250,000. Therefore, the No. 4 mesh scheme is found to be a good trade-off between numerical accuracy and computational cost.

As is plotted in Fig. 3(a), the time- and area-averaged surface superheat is higher than the experimental data by 16%, while the time-averaged superheat value based on localized temperature measurements is lower than that obtained in experiments by 8%. This is because the heating wall temperature located at corners near side walls are significantly higher than that under the central flatten vapor core, as shown in Fig. 3(b).

3.3. Validation with experimental data

Experimental studies have been performed to obtain annular flow boiling data in a narrow microchannel, which is used to validate our numerical methods [43].

The test flow loop for saturated flow boiling consists of a storage tank, a mass flowmeter, a particle filter, two preheaters, a microchannel test section, a high-speed camera, a condenser and three pumps, as shown in Fig. 4. The mass flowmeter provides a constant flow rate of deionized water. A 7-μm particle filter is located before preheaters, which are used to heat up the water to the required inlet quality and temperature. Detailed information of the microchannel test module assembly can be found in our previous study [43].

Comparison of numerical results and experimental data at various mass fluxes and heat fluxes is plotted in Fig. 5. It can be seen in Fig. 5(a) that the average heat transfer coefficients over the heating wall with different mass fluxes show good agreement with experimental data for all numerical cases. It should be noted that the

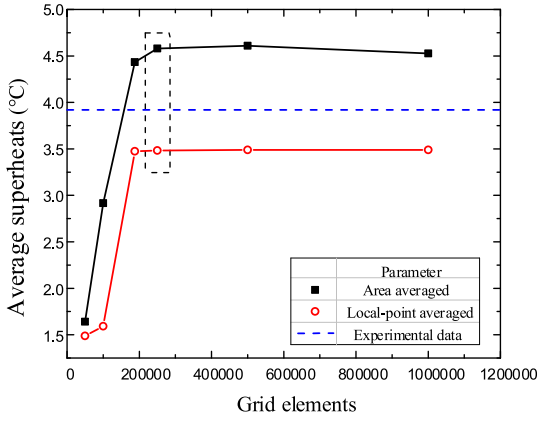

(a)

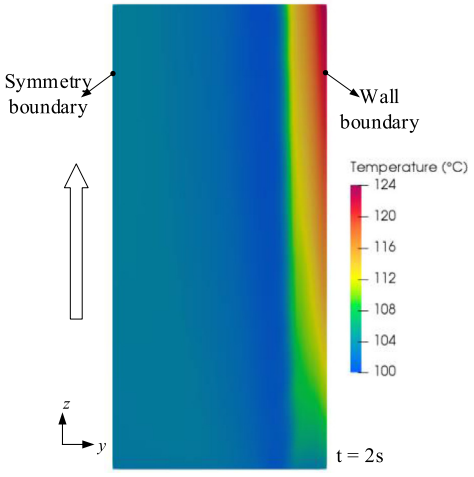

(b)

Fig. 3. (a) Simulation results of mesh independence test (b) temperature profile on the heating wall when the flow and heat transfer reach a quasi-steady state (not to scale, with 5 times magnification in y-direction).

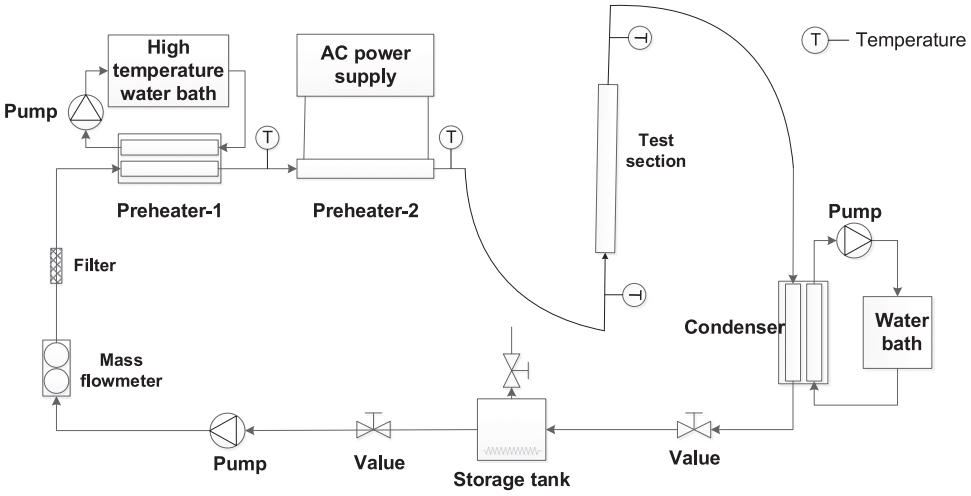

Fig. 4. Schematic of experimental microchannel flow loop for flow boiling.

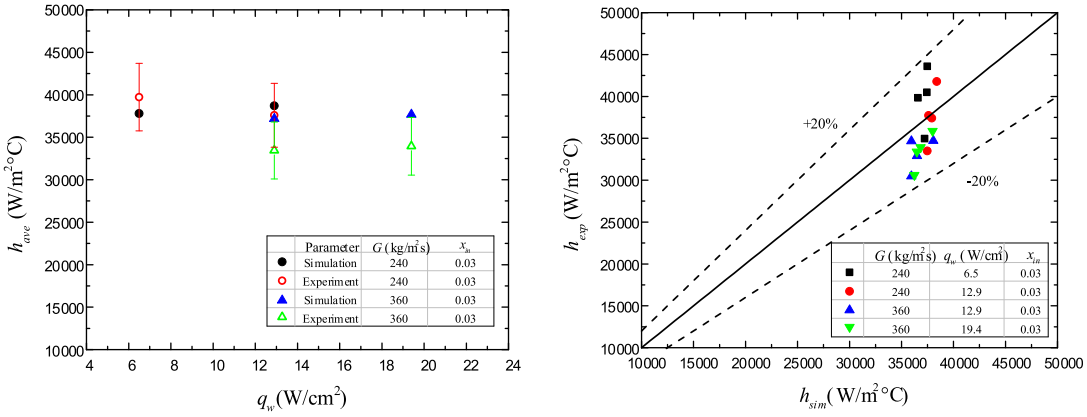

(a) Average heat transfer coefficients vs. wall heat flux

(b) Experimental heat transfer coefficients vs. numerical heat transfer coefficients

Fig. 5. Comparison between simulation results and experimental data. (a) Average heat transfer coefficients vs. wall heat flux, (b) Experimental heat transfer coefficients vs. numerical heat transfer coefficients.

values of heat transfer coefficient are time- and area-averaged after the flow reaches the quasi-steady state ($t > 1$ s). The total flow time simulated was 2 s and thus the numerical data for comparison is calculated with simulated time ranging from 1 s to 2 s. The experimental uncertainty in heat transfer coefficients is ±10%, as detailed in Fig. 5(a). When the mass flow rate increases, the numerical average heat transfer coefficients decline slightly, which is reasonably consistent with the experimental trend. As shown in Fig. 5(b), all average heat transfer coefficients obtained at the four localized measurement points in the flow direction lie within a ±20% error band of the experimental results.

4. Results and discussion

4.1. Case setup

The effects of variable parameters including wall heat flux q_w, inlet mass flux G and inlet quality x_{in} on annular flow boiling heat transfer characteristics in the single rectangular microchannel with large width-to-depth ratio have been discussed in this section. Eight cases are tested in this section and the operating conditions of them are extended from the aforementioned validation cases, as detailed in Table 3.

Table 3
Case setup.

Case No.	G (kg/m^{2}s)	q_w (W/cm^2)	x_{in}	$u_{in,v}$	$u_{in,l}$
1	240	6.7	0.03	13.84	1.51
2	240	13.3	0.03	13.84	1.51
3	240	20.0	0.03	13.84	1.51
4	240	6.7	0.05	22.19	1.86
5	240	6.7	0.07	30.38	2.16
6	360	6.7	0.03	20.76	2.27
7	360	13.3	0.03	20.76	2.27
8	360	20.0	0.03	20.76	2.27

4.2. Heat transfer characteristics

Fig. 6 shows the simulation results of time-averaged local heat transfer coefficient along z-direction on heating wall with various imposed wall heat flux and different mass fluxes. In Fig. 6(a), when the wall heat flux increases, the time-averaged heat transfer coefficient increases gradually, which has been illustrated in the literature. Because dryout of flow boiling is not observed during our numerical results, so the heat transfer characteristics of annular flow show a great dependence on the temperature gradient profiles in the surrounding liquid film of the vapor core, which is inversely proportional to liquid film thickness. With increments of wall heat

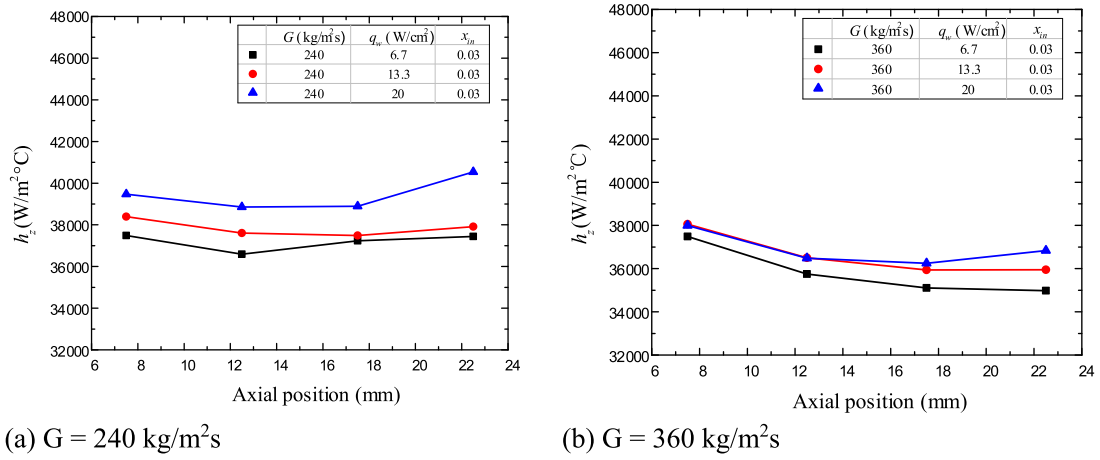

Fig. 6. Effect of heat flux on local heat transfer coefficients along the flow length with different mass fluxes, (a) G = 240 kg/m^{2}s, (b) G = 360 kg/m^{2}s.

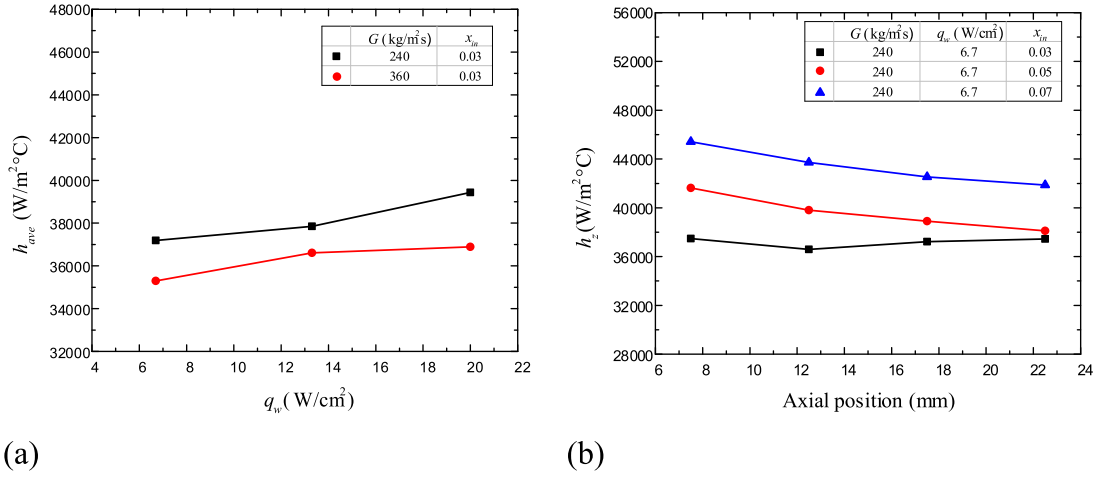

Fig. 7. (a) Effect of mass flux on average heat transfer coefficients in terms of the wall heat flux (b) effect of inlet vapor quality on local heat transfer coefficients along the flow length.

flux, the annular liquid film entrained between the central vapor column and the heating wall evaporates gradually due to boiling, leading to a larger temperature difference between the interface and the heating wall [34]. Moreover, the vapor phase velocity increases dramatically due to the vigorous vaporization and large liquid-vapor density ratio of water, which may cause flow perturbations and heat transfer enhancement. In addition, when the total inlet mass flux is 360 kg/m^{2}s, a slightly increase in time-averaged local heat transfer coefficient can also be observed when wall heat flux increases, as plotted in Fig. 6(b).

Fig. 7(a) plots the quasi-steady state time-averaged heat transfer coefficients obtained from simulation at various mass fluxes with wall heat flux as abscissa. It can be observed that larger inlet mass flux leads to lower wall heat transfer coefficient. For the two-phase annular flow in microscale, the interfacial shear stress determines the liquid-vapor interface distribution. Thus, increased superficial velocity of liquid phase results in the accumulation of the trapped liquid film under the vapor core [38]. Since the convective evaporation of the annular flow is the main heat dissipation method in the microchannel [56], the corresponding heat transfer performance will be suppressed by the increment of mass flux, as plotted in Fig. 7(a).

Local heat transfer coefficients are presented in Fig. 7(b) for different inlet vapor qualities. Heat transfer coefficients are predicted to increase with increasing inlet vapor quality in the narrow rectangular microchannel during annular flow boiling. The reason is that with constant mass and heat fluxes, liquid film thickness near the heating wall decreases with increasing inlet quality in annular flow [33].

4.3. Flow patterns

The liquid-vapor interface distribution (left) and velocity profile (right) at the plane of z = 15 mm from the front edge of the heated section is pictured in Fig. 8. The liquid phase (red region in the phase distribution diagram) tends to accumulate at the channel corners considering the impact of surface tension force. The interfacial Laplace pressure drop decreases near channel corners due to the large curvature of the liquid-vapor interface, thus more predominated surface tension would drive the local liquid supply to both sides of the channel. An elongated and convex shape of the liquid-vapor interface is therefore formed, which is significantly different from the axisymmetric interface distribution for annular flow regime in circular tubes [40]. As a consequence, a minimum value of the surrounding liquid film thickness appeared somewhere close to the channel corners, which is in accordance with the results of the mathematical or numerical studies of annular flow inside rectangular or flatten channels in the literature [27,38,40].

Fig. 8 shows that variation of mass flux has little effect on the cross-sectional liquid-vapor phase distribution. When mass flux increases, the central vapor column extends towards side walls

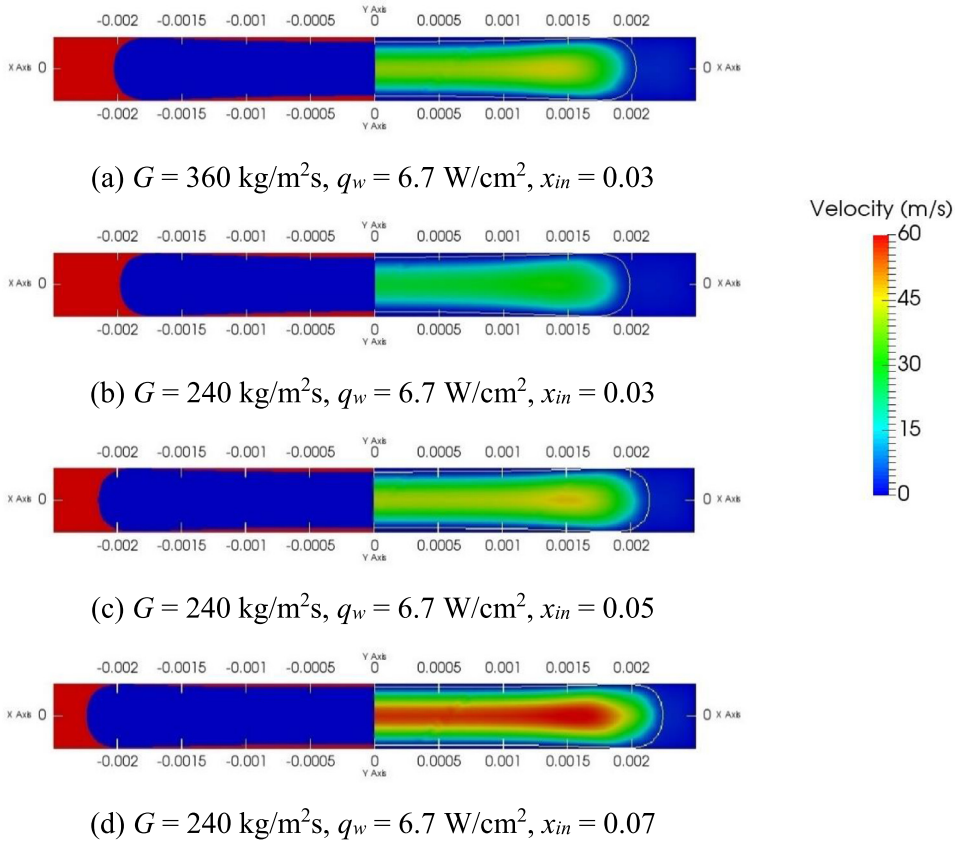

Fig. 8. Cross-sectional phase interface and velocity field distribution during saturated boiling in the rectangular superhydrophilic microchannel at t = 2 s. (a) G = 360 kg/m^{2}s, q_w = 6.7 W/cm^2, x_{in} = 0.03, (b) G = 240 kg/m^{2}s, q_w = 6.7 W/cm^2, x_{in} = 0.03, (c) G = 240 kg/m^{2}s, q_w = 6.7 W/cm^2, x_{in} = 0.05, (d) G = 240 kg/m^{2}s, q_w = 6.7 W/cm^2, x_{in} = 0.07.

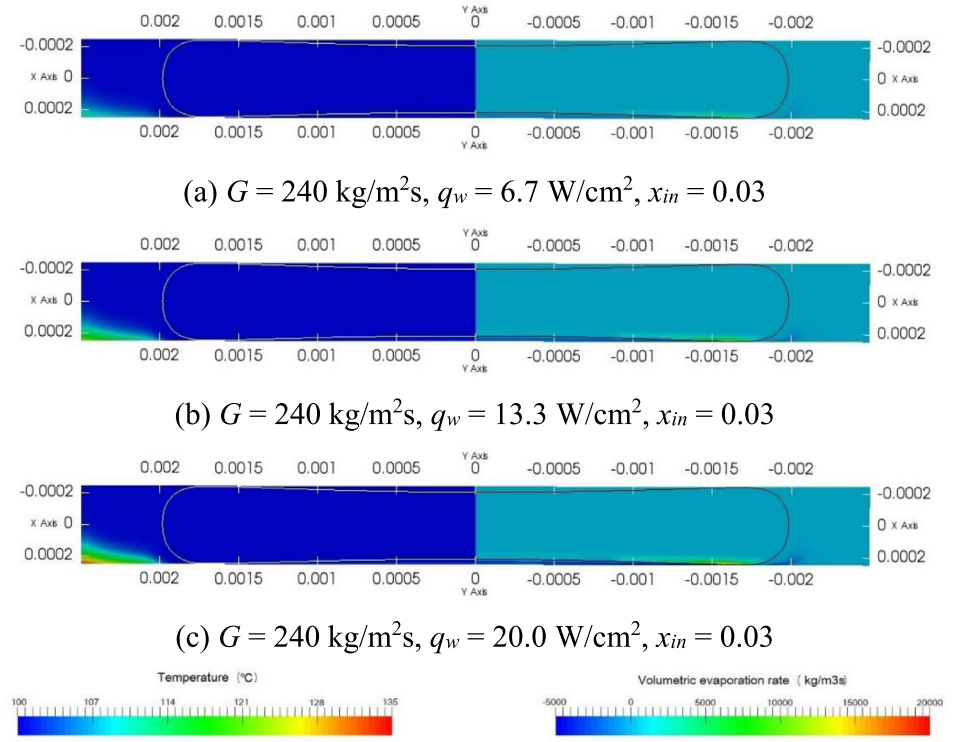

Fig. 9. Cross-sectional temperature profile and volumetric evaporation rate distribution (z = 35 mm) at t = 2 s. (a) G = 240 kg/m^{2}s, q_w = 6.7 W/cm^2, x_{in} = 0.03, (b) G = 240 kg/m^{2}s, q_w = 13.3 W/cm^2, x_{in} = 0.03, (c) G = 240 kg/m^{2}s, q_w = 20.0 W/cm^2, x_{in} = 0.03.

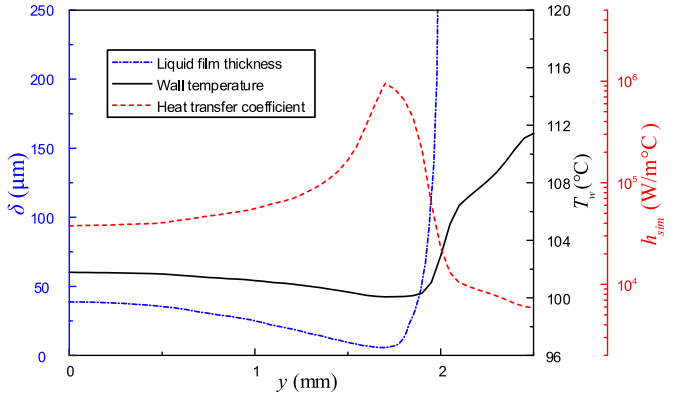

Fig. 10. Wall temperature and local heat transfer coefficient distribution along the y-direction (G = 240 kg/m^{2}s, q_w = 6.7 W/cm^2, x_{in} = 0.03, z = 35 mm, t = 2 s).

slightly in the transverse direction, leading to the increase of the liquid film thickness upon the heating wall as well as the decrease of heat transfer performance. Velocity of vapor phase is one or two orders of magnitude greater than that of liquid phase. At the cross-sectional plane, velocity and void fraction of the central vapor column are shown to increase with increasing inlet quality. As a result, the average heat transfer coefficient increases with decreasing liquid film thickness.

The temperature profile (left) and the volumetric phase-change source term distribution (right) is presented in Fig. 9, with solid line representing the interface. The liquid-vapor interface distribution in the channel cross section is almost unchanged as the imposed wall heat flux increases. Since the interfacial temperature is set to the saturation temperature by our phase change model, the temperature gradient between the heating wall and the interface becomes large when the wall heat flux increases. Besides, density source term in liquid side is negative while positive values are observed in the vapor phase region. The reason is that in saturated flow boiling, superheated liquid is transformed into saturated vapor phase according to our phase model.

Fig. 10 illustrates the local wall temperature and local heat transfer coefficient along the x direction at the plane of z = 35 mm on the heating wall. The liquid film thickness is also plotted in the figure to explain the trends of temperature and heat transfer coefficient. It can be found that the liquid film thickness reaches a minimum value when y = ~1.7 mm, resulting from the effect of surface tension and interfacial shear stress [57]. The wall temperature on the heating wall declines gradually along x-direction and reaches a minimum value when the liquid film thickness is at the minimum point. At the same time the wall heat transfer coefficient is maximized because the difference between the wall temperature and the saturation temperature is quite small. Since the liquid film disappears near the channel corners (2 mm $< x <$ 2.5 mm), the local heat transfer coefficient decreases dramatically to about 10^4 W/m^2°C and the wall superheat reaches around 8 °C.

5. Conclusion

Numerical investigation on hydrodynamics and thermodynamics of annular flow boiling in a rectangular microchannel with large width-to-depth ratio is performed in the present study. Saturation temperature recovery model based on the VOF method is adopted to explore heat transfer characteristics in a three-dimensional computational domain. Main conclusions are summarized as follows:

1) Validation of our methods for saturated annular flow boiling has been conducted by comparing the numerical results with experimental data of our research group acquired in a nano-silica coated superhydrophilic microchannel. Average wall superheats and heat transfer coefficients of numerical simulations show good agreement with experimental data at various operating conditions.
2) Increasing the wall heat flux or inlet vapor quality will decline the thickness of liquid film, and hence the heat transfer coefficient of annular flow boiling will increase. Furthermore, when the wall heat flux is fixed, the heat transfer coefficient of the channel decreases when the mass flux is increased.
3) A convex shape of the liquid-vapor interface is formed due to dominated surface tension force. The increase in the inlet quality will increase the vapor phase velocity and the void fraction; but the liquid film thickness upon the heating wall will decrease due to the decreasing volume of liquid in the channel. Besides, the wall temperature underneath the central vapor core in the annular flow regime is relatively low when compared with that at the channel corner, which is caused directly by the uneven distribution of liquid film thickness.

Declaration of Competing Interest

The authors do not have any actual and potential conflict of interest with works and organizations described in the paper.

CRediT authorship contribution statement

Yang Luo: Conceptualization, Methodology, Software. **Wei Li:** Supervision. **Kan Zhou:** Data curation, Writing - original draft. **Kuang Sheng:** Visualization, Investigation. **Shuai Shao:** Visualization, Investigation. **Zhengjiang Zhang:** Writing - review & editing. **Jingcai Du:** Writing - review & editing. **W.J. Minkowycz:** Supervision.

Acknowledgments

This work was supported by the National Science Foundation of Zhejiang Province(LY19E060004).

Supplementary materials

Supplementary material associated with this article can be found, in the online version, at doi:10.1016/j.ijheatmasstransfer.2019.119246.

References

[1] T.G. Karayiannis, M.M. Mahmoud, Flow boiling in microchannels: Fundamentals and applications, Appl. Therm. Eng. 115 (2017) 1372–1397.
[2] W. Li, Z. Wu, A general correlation for adiabatic two-phase pressure drop in micro/mini-channels, Int. J. Heat Mass Transf. 53 (13-14) (2010) 2732–2739.
[3] W. Li, Z. Wu, A general criterion for evaporative heat transfer in micro/mini-channels, Int. J. Heat Mass Transf. 53 (9-10) (2010) 1967–1976.
[4] W. Li, Z. Wu, A general correlation for evaporative heat transfer in micro/mini-channels, Int. J. Heat Mass Transf. 53 (9-10) (2010) 1778–1787.
[5] W. Li, Z. Wu, Generalized adiabatic pressure drop correlations in evaporative micro/mini-channels, Exp. Therm. Fluid Sci. 35 (6) (2011) 866–872.
[6] Z. Wu, W. Li, S. Ye, Correlations for saturated critical heat flux in microchannels, Int. J. Heat Mass Transf. 54 (1-3) (2011) 379–389.
[7] E. Costa-Patry, J.R. Thome, Flow pattern-based flow boiling heat transfer model for microchannels, Int. J. Refrig. 36 (2) (2013) 414–420.
[8] J. Thome, A. Bar-Cohen, R. Revellin, I. Zun, Unified mechanistic multiscale mapping of two-phase flow patterns in microchannels, Exp. Therm. Fluid Sci. 44 (-) (2013) 1–22.
[9] T. Harirchian, S.V. Garimella, Microchannel size effects on local flow boiling heat transfer to a dielectric fluid, Int. J. Heat Mass Transf. 51 (15) (2008) 3724–3735.
[10] T. Harirchian, S.V. Garimella, The critical role of channel cross-sectional area in microchannel flow boiling heat transfer, Int. J. Multiph. Flow 35 (10) (2009) 904–913.
[11] T. Harirchian, S.V. Garimella, Boiling heat transfer and flow regimes in microchannels—a comprehensive understanding, J. Electron. Packag. 133 (1) (2011) 011001–011001-011010.

[12] T. Alam, P.S. Lee, C.R. Yap, L. Jin, A comparative study of flow boiling heat transfer and pressure drop characteristics in microgap and microchannel heat sink and an evaluation of microgap heat sink for hotspot mitigation, Int. J. Heat Mass Transf. 58 (1-2) (2013) 335–347.
[13] Z.J. Edel, A. Mukherjee, Experimental investigation of vapor bubble growth during flow boiling in a microchannel, Int. J. Multiph. Flow 37 (10) (2011) 1257–1265.
[14] D. Bogojevic, K. Sefiane, G. Duursma, A. Walton, Bubble dynamics and flow boiling instabilities in microchannels, Int. J. Heat Mass Transf. 58 (1-2) (2013) 663–675.
[15] H. Huang, N. Borhani, J.R. Thome, Thermal response of multi-microchannel evaporators during flow boiling of refrigerants under transient heat loads with flow visualization, J. Electron. Packag. 138 (3) (2016) 031004.
[16] S. Bigham, A. Fazeli, S. Moghaddam, Physics of microstructures enhancement of thin film evaporation heat transfer in microchannels flow boiling, Sci. Rep. 7 (-) (2017) 44745.
[17] B. Wang, M. He, H. Wang, H. Qiu, Flow boiling heat transfer in wettability patterned microchannels, in: IEEE Intersociety Conference on Thermal and Thermomechanical Phenomena in Electronic Systems IEEE, Orlando, FL, USA, 2017, pp. 759–766.
[18] M. Piasecka, K. Strąk, B. Maciejewska, Calculations of flow boiling heat transfer in a minichannel based on Liquid Crystal and Infrared Thermography data, Heat Transf. Eng. 38 (3) (2017) 332–346.
[19] W.H. Lee, A pressure iteration scheme for two-phase flow modelling, in: T.N Veziroglu (Ed.), Multiphase Transport Fundamentals, Reactor Safety, Applications, Hemisphere, Washington, DC, 1980, pp. 61–82.
[20] Z. Yang, X. Peng, P. Ye, Numerical and experimental investigation of two phase flow during boiling in a coiled tube, Int. J. Heat Mass Transf. 51 (5-6) (2008) 1003–1016.
[21] L. Yang, A. Guo, W. Zhang, Computational fluid dynamics simulation of subcooled flow boiling in vertical rectangular 2-mm narrow channel, Adv. Mech. Eng. 7 (7) (2015) 1–12.
[22] A. Mukherjee, S.G. Kandlikar, Numerical simulation of growth of a vapor bubble during flow boiling of water in a microchannel, Microfluid. Nanofluid. 1 (2) (2005) 137–145.
[23] A. Mukherjee, S. Kandlikar, Z. Edel, Numerical study of bubble growth and wall heat transfer during flow boiling in a microchannel, Int. J. Heat Mass Transf. 54 (15-16) (2011) 3702–3718.
[24] R. Zhuan, W. Wang, Flow pattern of boiling in micro-channel by numerical simulation, Int. J. Heat Mass Transf. 55 (5-6) (2012) 1741–1753.
[25] A.S. Rattner, S. Garimella, Simple mechanistically consistent formulation for Volume-of-Fluid based computations of condensing flows, J. Heat Transf. 136 (7) (2014) V08.
[26] Y. Luo, J. Zhang, W. Li, E. Sokolova, Y. Li, W. Minkowycz, Numerical investigation of the bubble growth in horizontal rectangular microchannels, Numerical Heat Transfer, Part A 71 (12) (2017) 1175–1188.
[27] A. Ferrari, M. Magnini, J.R. Thome, Numerical analysis of slug flow boiling in square microchannels, Int. J. Heat Mass Transf. 123 (-) (2018) 928–944.
[28] D. Lorenzini, Y.K. Joshi, Computational fluid dynamics modeling of flow boiling in microchannels with nonuniform heat flux, J. Heat Transf. 140 (1) (2017) 011501.
[29] J. Thome, V. Dupont, A.M. Jacobi, Heat transfer model for evaporation in microchannels. Part I: presentation of the model, Int. J. Heat Mass Transf. 47 (14-16) (2004) 3375–3385.
[30] L. Zhang, J. Koo, L. Jiang, M. Asheghi, K.E. Goodson, J.G. Santiago, T.W. Kenny, Measurements and modeling of two-phase flow in microchannels with nearly constant heat flux boundary conditions, J. Microelectromech. Syst. 11 (1) (2002) 12–19.
[31] W. Qu, I. Mudawar, Flow boiling heat transfer in two-phase micro-channel heat sinks—-I. Experimental investigation and assessment of correlation methods, Int. J. Heat Mass Transf. 46 (15) (2003) 2755–2771.
[32] R.K. Sarangia, A. Bhattacharyaa, R.S. Prasherb, Numerical modelling of boiling heat transfer in microchannels, Appl. Therm. Eng. 29 (2) (2009) 300–309.
[33] A. Megahed, I. Hassan, Analytical modeling of annular flow boiling heat transfer in mini- and microchannel heat sinks, J. Heat Transf.-Transact. ASME 132 (4) (2010) 041012.
[34] Y.W. Na, J. Chung, Two-phase annular flow and evaporative heat transfer in a microchannel, Int. J. Heat Fluid Flow 32 (2) (2011) 440–450.
[35] Z. Guo, B. Haynes, D. Fletcher, Numerical simulation of annular flow boiling in microchannels, J. Comput. Multiph. Flows 8 (1) (2016) 61–82.
[36] Z. Guo, D.F. Fletcher, B.S. Haynes, Numerical simulation of annular flow hydrodynamics in microchannels, Comput. Fluids 133 (2016) 90–102.
[37] S. Jesseela, C. Sobhan, Numerical modeling of annular flow with phase change in a microchannel, Int. J. Therm. Sci. 89 (2015) 87–99.
[38] R.S. Patel, J.A. Weibel, S.V. Garimella, Mechanistic modeling of the liquid film shape and heat transfer coefficient in annular-regime microchannel flow boiling, Int. J. Heat Mass Transf. 114 (-) (2017) 841–851.
[39] W. Li, Y. Luo, J. Zhang, W.J. Minkowycz, Simulation of single bubble evaporation in microchannel in zero gravity with thermocapillary effect, J. Heat Transf. 140 (11) (2018) 112403.
[40] W. Li, J. Zhang, G. Bai, J.-l Xu, T.W Simon, J Li, J.-j. Wei, Numerical simulation of condensation for R410A in horizontal round and flattened minichannels, J. Heat Transf. 139 (2) (2017) 021501.
[41] K. Zhou, C. Coyle, J. Li, J. Buongiorno, W. Li, Flow boiling in vertical narrow microchannels of different surface wettability characteristics, Int. J. Heat Mass Transf. 109 (-) (2017) 103–114.
[42] W. Li, J. Li, Z. Feng, K. Zhou, Z. Wu, Local heat transfer in subcooled flow boiling in a vertical mini-gap channel, Int. J. Heat Mass Transf. 110 (-) (2017) 796–804.
[43] W. Li, K. Zhou, J. Li, Z. Feng, H. Zhu, Effects of heat flux, mass flux and two-phase inlet quality on flow boiling in a vertical superhydrophilic microchannel, Int. J. Heat Mass Transf. 119 (2018) 601–613.
[44] H.G. Weller, G. Tabor, H. Jasak, C Fureby, A tensorial approach to computational continuum mechanics using object-oriented techniques, Comput. Phys. 12 (6) (1998) 620–631.
[45] M. Nabil, A.S. Rattner, Inter thermal phase change foam—A framework for two-phase flow simulations with thermally driven phase change, SoftwareX 5 (2016) 216–226.
[46] H. Marschall, K. Hinterberger, C. Schüler, F. Habla, O. Hinrichsen, Numerical simulation of species transfer across fluid interfaces in free-surface flows using OpenFOAM, Chem. Eng. Sci. 78 (2012) 111–127.
[47] A.S. Rattner, S. Garimella, Taylor flow in intermediate diameter channels: Simulation and hydrodynamic models, Int. J. Heat Mass Transf. 103 (2016) 1108–1124.
[48] J.U. Brackbill, D.B. Kothe, C. Zemach, A continuum method for modeling surface tension, J. Comput. Phys. 100 (2) (1992) 335–354.
[49] W.H. Lee, Pressure iteration scheme for two-phase flow modeling, IN" MULTIPHASE TRANSPORT: FUNDAMENTALS, REACTOR SAFETY, APPLICATIONS". (1980) 407–432.
[50] F. Gibou, L. Chen, D. Nguyen, S. Banerjee, A level set based sharp interface method for the multiphase incompressible Navier–Stokes equations with phase change, J. Comput. Phys. 222 (2) (2007) 536–555.
[51] R.W. Schrage, A Theoretical Study of Interphase Mass Transfer, Columbia University Press, 1953.
[52] S.-J. Kim, G.-C. Park, Interfacial heat transfer of condensing bubble in subcooled boiling flow at low pressure, Int. J. Heat Mass Transf. 54 (13-14) (2011) 2962–2974.
[53] A.S. Rattner, S. Garimella, Simple mechanistically consistent formulation for volume-of-fluid based computations of condensing flows, J. Heat Transf. 136 (7) (2014) 071501.
[54] A. Cioncolini, J.R. Thome, Void fraction prediction in annular two-phase flow, Int. J. Multiph. Flow 43 (-) (2012) 72–84.
[55] R. Gupta, D.F. Fletcher, B.S. Haynes, On the CFD modelling of Taylor flow in microchannels, Chem. Eng. Sci. 64 (12) (2009) 2941–2950.
[56] R. Zhuan, W. Wang, Boiling heat transfer characteristics in a microchannel array heat sink with low mass flow rate, Appl. Therm. Eng. 51 (1-2) (2013) 65–74.
[57] Y. Ding, L. Jia, L. Yin, Y. Zhang, Z. An, Theoretical investigation on convective condensation annular flow of R410a inside rectangular microchannel, Int. J. Heat Mass Transf. 131 (2019) 698–708.